Available online at www.sciencedirect.com
ScienceDirect
Catalysis Today 126 (2007) 18–26
CATALYSIS TODAY
www.elsevier.com/locate/cattod

Design and operation of a high pressure reaction cell for in situ X-ray absorption spectroscopy

Simon R. Bare [a,*], Ning Yang [b,1], Shelly D. Kelly [c], George E. Mickelson [a], Frank S. Modica [a]

[a] *UOP LLC, Des Plaines, IL 60016, USA*
[b] *Argonne National Laboratory, Argonne, IL 60439, USA*
[c] *EXAFS Analysis, Bolingbrook, IL 60439, USA*

Available online 21 November 2006

Abstract

X-ray absorption spectroscopy measurements of catalytic reactions have been instrumental in advancing the understanding of catalytic processes. These measurements require an in situ catalysis reaction cell with unique properties. Here we describe the design and initial operation of an in situ/operando catalysis reaction cell for transmission X-ray absorption spectroscopy measurements. The cell is designed: to be an ideal catalytic reactor with no mass transfer effects; to give the same conversion and selectivity under similar space velocities as standard laboratory micro-reactors; to be operational temperatures up to 600 °C and pressures up to 14 bar; to be X-ray transparent allowing XAS measurement to be collected in transmission for all elements with $Z \geq 23$ (vanadium K-edge at 5.5 keV); to measure the actual catalyst bed temperature; to not use o-ring seals, or water cooling; to be robust, compact, easy to assemble, and use, and relatively low cost to produce. The heart of the cell is fabricated from an X-ray transparent beryllium tube that forms a plug flow reactor. XAFS data recorded during the reduction of a Re/γ-Al_2O_3 catalyst as a function of hydrogen pressure from 0.05 to 8 bar, and from a Pt–Sn/γ-Al_2O_3 catalyst during *n*-heptane reforming are given as initial examples of the versatility of the reactor.

Keywords: X-ray absorption; In situ spectroscopy; Catalysis

1. Introduction

There is a continuous growing trend in the catalysis community to use X-ray absorption fine structure (XAFS) spectroscopy to study heterogeneous catalysts. Typically, XAFS is used to determine the average local atomic and electronic structure of the metal site(s) during a heterogeneous catalytic reaction. The structure of the catalyst is probed while the catalytic performance is simultaneously measured using an appropriate on-line analytical technique, e.g. gas chromatography, residual gas analysis or FTIR. This experimental procedure has been called in situ XAFS or operando XAFS. To facilitate the understanding of catalytic properties, materials are often prepared using different synthetic methods that result in different selectivity and/or conversion for the particular reaction being studied. If these activity data can be correlated with structural data obtained by operando XAFS, then so called structure-activity relationships are formed (see for example Refs. [1–5]). In this manner, the change in activity can be correlated with a change in structure, which will then provide clues as to the active reaction site. The ‘‘holy grail’’ is to be able to identify the active metal site and to specifically design its function into an improved catalyst.

In order to collect in situ XAFS data, an appropriate reaction cell must be designed and fabricated because to our knowledge, no commercial reaction cells are available. This has resulted in many publications of in situ catalysis XAFS cell designs. Each of these designs has certain advantages and disadvantages and the choice is often determined by a combination of X-ray energy range, type of detection scheme, pressure and temperature limitations, catalyst type, information desired, and others [6–16]. It is clear that these cell designs always

* Corresponding author. Tel.: +1 847 391 3171; fax: +1 847 391 3719.
E-mail address: simon.bare@uop.com (S.R. Bare).
URL: http://www.uop.com
[1] Present address: BRUKER AXS Inc., Madison, WI 53711, USA.

0920-5861/$ – see front matter © 2006 Elsevier B.V. All rights reserved.
doi:10.1016/j.cattod.2006.10.007

involve a compromise between optimum catalytic conversion, design, engineering design and optimum spectroscopy design: it is relatively easy to build a cell that is a true plug flow reactor, and it is easy to fabricate a cell that is ideal for XAFS. However, to wed these two usually leads to a compromise. It is also clear that no one design is *a priori* better than another, it all depends on the application, and the information that is desired.

The "capillary cell" design, the subject of this paper, is in use by several catalysis research groups. This in situ cell design is a reactor that is a true plug flow reactor, and as such exhibits preferable mass transfer characteristics [3]. The initial design was published by Clausen et al. [9,10], and has since been implemented by other research groups [8,11,17,18]. The original design of Clausen used a quartz capillary with a wall thickness of 10 μm. This type of thin-wall capillary tube is commonly used by the X-ray diffraction community. Meitzner reports using a quartz capillary with a wall thickness of 0.2 mm—which limits the practical usable X-ray energy range to energies >10 kV [16]. A modification on the concept by Frenkel and co-workers [13] is the use of Kapton® tubing for improved X-ray transmission especially at lower energies, but at the expense of a maximum working temperature of 400 °C [19]. The requirements for the cell design reported here were: (i) an ideal catalytic reactor with no mass transfer effects, (ii) a reactor that gives the same conversion and selectivity under similar space velocities as standard laboratory micro-reactors, (iii) operable at temperatures up to 600 °C and pressures up to 14 bar, (iv) X-ray transparent to allow XAFS data to be collected in transmission for all elements with $Z \geq 23$ (vanadium K-edge at 5.5 keV), (v) actual catalyst bed temperature measured, (vi) no o-ring seals, (vii) no water cooling, (viii) robust, easy to assemble and use, (ix) compact, and (x) relatively low cost. These design requirements have either been met or exceeded with the use of a capillary-type cell fabricated from PF60 grade beryllium.

To demonstrate the capability of the in situ XAFS cell we will give two examples: (a) a study of the effect of hydrogen pressure on the reduction temperature of a Re/γ-alumina catalyst, and (b) in situ XAFS data from a Pt–Sn/γ-Al_2O_3 bimetallic reforming catalyst where true operando XAFS data were recorded during the reforming of *n*-heptane.

The structural characterization of rhenium oxide supported on γ-Al_2O_3, and it reduction to give small Re clusters, has been studied primarily by EXAFS, laser Raman and FTIR. There is consensus in the literature that after impregnation of the alumina with perrhenic acid or ammonium perrhenate, drying and calcining that below monolayer coverage, the rhenium oxide species is present as an atomically dispersed perrhenate species, $[ReO_4]^-$, with the Re in the +7 oxidation state [20,21]. The reduction of the rhenium oxide species has also been studied (see e.g. Ref. [22], and references therein) by classical TPR techniques. For the purposes of this paper, the key parameter affecting the temperature of reduction is the hydrogen partial pressure. It has been reported that the temperature of reduction, T_{max}, shifts to lower temperature by 220 °C (from 550 to 330 °C) as the hydrogen pressure is increased from 0.05 bar to 1 bar [23]. However, there are no publications that show the effects of hydrogen pressure on the reduction temperature at pressured greater than 1 bar. In this paper we extend the effects of hydrogen pressure on the reduction to 8 bar, and show that above 1 bar there is only an additional small shift in the reduction temperature.

The characterization of PtSn supported on alumina has been well studied by many techniques including XAFS [24–26]. All of these EXAFS studies were recorded after hydrogen reduction (the normal activation procedure for such a catalyst) but with the catalyst cooled to sub-ambient temperatures for the data collection. The conclusions from these studies are that there is substantial interaction between Pt and Sn. Meitzner et al. [24] proposed that the morphology is small Pt clusters dispersed on the alumina containing Sn^{2+} at the surface. A similar conclusion was reached by Caballero et al. [25]. In comparison Borgna et al. [26] concluded that there is a mixture of pure Pt clusters and Pt–Sn clusters present after hydrogen reduction up to 500 °C for Pt–Sn on silica. In this paper it is shown that Pt–Sn clusters are formed, and that it is likely that the Sn is not fully reduced. Also, within the accuracy of the current data, the cluster chemistry is similar in both a pure hydrogen atmosphere and in a hydrogen/heptane flow at elevated temperature.

2. Experimental

2.1. XAFS measurements

XAFS data were collected at beamline 33-BM-B at the Advanced Photon Source, Argonne National Laboratory, with some initial testing at X18B at the National Synchrotron Light Source, Brookhaven National Laboratory. At the NSLS the energy of the electron in the storage ring is 2.5 GeV with a ring current of 60–150 mA. The Si(1 1 1) monochromator was detuned 30% to minimize the content of the higher harmonics incident on the sample. The APS storage ring was operated at 7 GeV with a constant ring current of 105 mA. A double crystal monochromator with Si(1 1 1) crystals was used to select the incident X-ray energy. Harmonics were removed by two Rh-coated mirrors, with the first mirror also acting as a collimator. If the cell is operated in the horizontal arrangement, then the geometry of the cell (tubular reactor) demands that the X-ray beam be narrow in the vertical direction to ensure that the path length probed by the beam is uniform. This is achieved either by using a narrow monochromator exit slit, or using vertical focusing optics (e.g. mirror), or a combination of the two. At X18B a narrow slit was used (0.1 mm vertical height), while at 33-BM advantage was taken of the vertical-focusing mirror to achieve a vertical beam height of around 0.2 mm, followed by a 0.1 mm exit slit to further define the geometry.

XAFS data reduction and analysis were performed using Athena and Artemis [27] which are an interface to IFEFFIT [28]. The background was removed from each data set and then the resulting $\chi(k)$ data were averaged using standard procedures. The data were fit in R-space with theoretical models constructed from Feff [29].

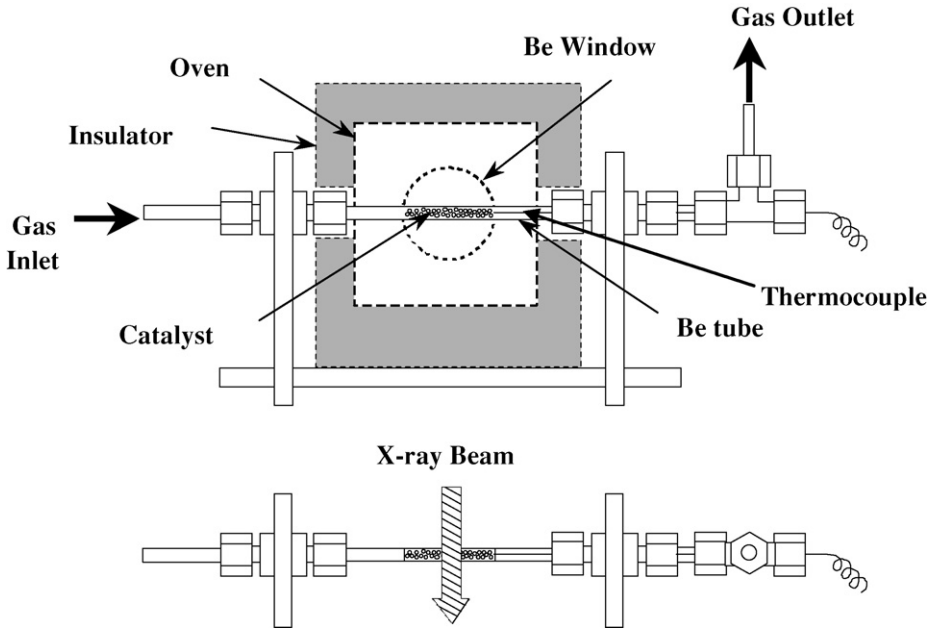

Fig. 1. Schematic of the layout of the Be tube XAFS reactor. The main components are labeled.

2.2. Catalyst preparation

The 0.7 wt.% Re/γ-alumina catalyst was prepared by evaporative impregnation of rhenium using ammonium perrhenate solution on a commercial zeolite/alumina extrudate (75% mordenite (MOR) and 25% γ-Al_2O_3). After the impregnation the catalyst was calcined in dry air at 540 °C for two hours. The Pt–Sn/γ-alumina catalyst had a loading of 0.35 wt.% Pt and 0.3 wt.% Sn. The catalyst and was prepared using standard methods. The metals loading of the catalysts were determined by ICP.

2.3. XAFS catalytic reactor cell design

The design is based on a tube fabricated from PF-60 grade beryllium [30] as the X-ray transparent reactor that houses the ground and meshed catalyst. In many respects beryllium is the ideal material for the fabrication of a catalytic reactor. It is very stiff, has very low density, has excellent thermal conductivity, a moderate coefficient of thermal expansion, can be machined, and is very stable mechanically and thermally. It also retains useful properties at both elevated and cryogenic temperatures. However, it does require a few special handling requirements that are well documented (for environmental safety and health information on beryllium, see Ref. [31]). Due to the low absorption cross-section of Be, the wall thickness of the Be tube can be made significantly thicker than, for example, a quartz tube. Over the typical XAFS energy range of 5–25 kV the absorption of 1.5 mm of beryllium is similar to that of 0.04 mm of quartz. The result is that a tube fabricated with 0.75 mm wall thickness of Be, which is strong and easy to handle, can be used instead of the somewhat fragile 20 μm wall thickness quartz tube. The use of beryllium as an X-ray transparent material for high pressure applications is not new, and has been well-documented (see for examples Refs. [32–34]). However, what is unique in this work is the fact that the whole reactor is fabricated from Be and not just the window material.

The overall catalytic reactor design is shown schematically in Fig. 1, and a photograph of the assembled reactor on a translation stage at the beamline ready for operation is shown in Fig. 2.

We have used two different sizes of Be tubes, supplied by Brush Wellman, depending upon the application. These tubes are both 10 cm long with an outside diameter of either 3.5 mm or 3.0 mm, each with a wall thickness of 0.75 mm, giving inside diameter of 2.0 mm and 1.5 mm, respectively. The tube diameter and wall thickness are chosen as a compromise among typical path lengths for common supported metal catalyst, X-ray transparency over a wide energy range, and cost and ease of manufacture. The typical catalyst loading in the reactor is 75 mg of meshed catalyst particles, giving a bed

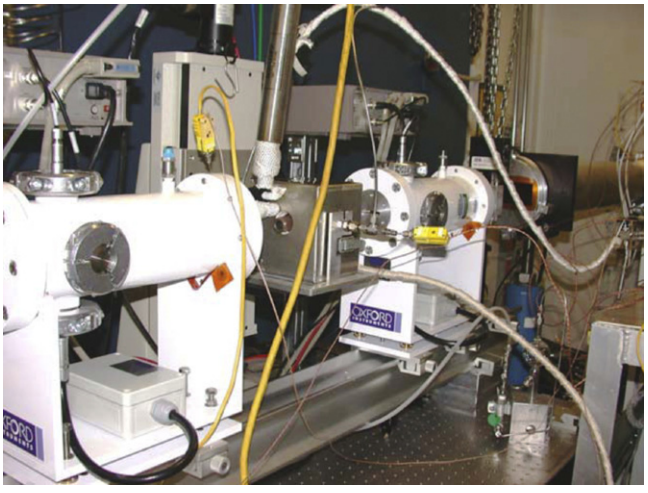

Fig. 2. Photograph of the fully assembled reactor at the beamline ready for operation.

depth of ∼12 mm. We have used mesh sizes of 60–80, 80–100 or 100–120 mesh (corresponding to particle sizes of 177–250 μm, 149–177 μm, and 125–149 μm, respectively). The seal to the Be tube is made using graphite ferrules in bulkhead compression fittings. One of the compression fittings is a ''tee''. The straight through part of the ''tee'' holds the thermocouple in place. The thermocouple, a type K dual thermocouple, is swaged such that it extends by 1–2 mm into the catalyst bed ensuring that the actual catalyst bed temperature is measured. The bulkhead fittings are used to hold the Be tube assembly rigidly inside an aluminum alloy frame as shown in Fig. 1. The frame has recessed holes drilled in its base plate to allow it to be rigidly bolted to a high precision *x*, *y*-translation stage that is typically found at most XAFS beamlines. Gas, supplied by 1/8 in. diameter stainless steel tubing, contacts the catalyst by flowing through the catalyst bed. The catalyst particles are held in place using quartz wool plugs at each end of the reactor.

The catalyst is heated using hot gas (nitrogen or air) using a custom-designed oven that fits around the Be tube reactor. The cylindrical oven has two standard pipe thread fittings arranged perpendicular to the Be tube. At the end of these fittings a thin Be foil (15.8 mm diameter, 0.254 mm thickness, PF-60 grade, vacuum tight) has been brazed to act as an X-ray transparent window through the oven walls. The extra 0.5 mm thickness of Be has minimal impact of the X-ray transparency at >10 keV. The oven is surrounded by ceramic insulation. The oven/insulation is held in place around the reactor by a stainless steel shroud with clasps welded to it to allow for rapid and easy assembly of the two halves. The assembled configuration is shown in Fig. 2.

The nitrogen is heated using a serpentine heater (Sylvania, Serpentine II housing assembly, with 3.6 kW two-stage heating element, 760 °C maximum operating temperature). The serpentine heater requires a positive flow of nitrogen to avoid overheating, burning out the heating element. A pressure switch is therefore used to ensure that there is indeed flow (the flow is controlled using a simple rotameter). Power to the heater itself is controlled via a PID loop using a Eurotherm controller (Model 2416). This arrangement has resulted in excellent temperature control during typical ramp and hold sequences, an example of which is shown in Fig. 3A. Fig. 3B shows examples of the linearity achieved using several different temperature ramps. At faster ramp rates (e.g. 20°/min) the upper temperature limit is around 400 °C, while using slower ramp rates, e.g. 2°/min, a temperature of 600 °C can achieved. It takes about 20 min for the reactor to cool from 600 °C to room temperature with the oven in place. We have also determined the temperature profile from one end of the reactor to the other. This was achieved by moving a temporary second thermocouple linearly through the catalyst bed while the bed was held at a constant temperature using the control loop from the first thermocouple. The 1/8 in. diameter stainless steel gas inlet and outlet lines are heat traced, and held at 110 °C. The measured temperature variation was 1.2 °C and 2 °C over ±10 mm from the center of the bed at a set-point of 300 °C and 450 °C, respectively. Thus the temperature profile along the axial length of the reactor is uniform.

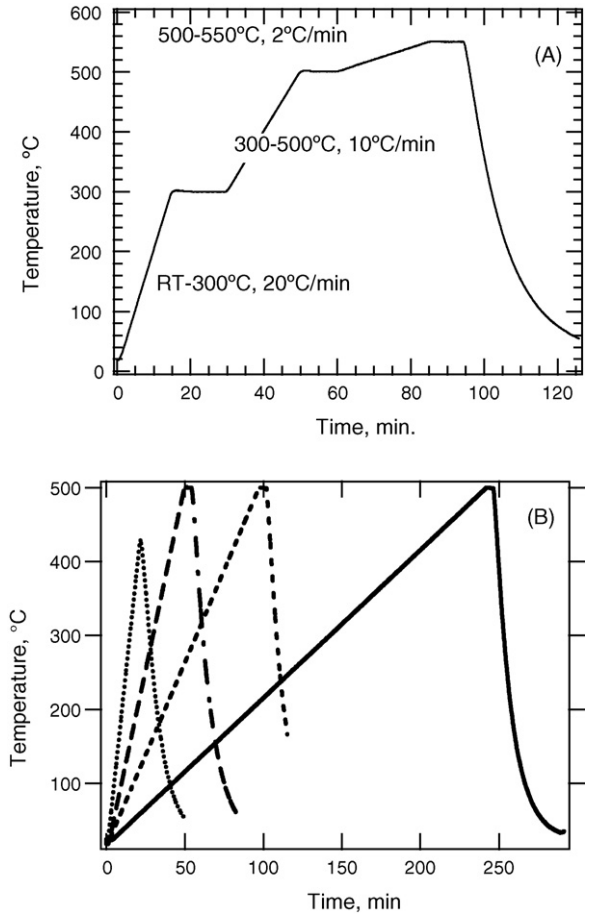

Fig. 3. A typical ramp and hold sequence recorded using the thermocouple embedded in the catalyst bed (A), and catalyst bed temperatures measured using embedded thermocouple during different ramp rates: 2°/min (solid), 5°/min (dashed), 10°/min (dot-dash) and 20°/min (dotted) (B).

2.4. Gas/liquid feed system and product analysis

The feed system to the reactor is modular and is mounted in a cabinet. This allows relatively easy movement and re-assembly of the system into a typical experimental X-ray hutch at a synchrotron beam line. The whole system is micro-processor controlled allowing full control of the gas atmosphere and pressure inside the reactor from the experimental control station outside the hutch. A schematic of the feed system is shown in Fig. 4. There are six mass flow controllers for gas feeds. Two of the mass flow controllers supply helium (low and high flow), one for hydrogen, one for 20% oxygen in helium, and two reserved for hydrocarbon or other gases. Each of these gases passes through appropriate gas purifiers (VICI Mat/Sen) mounted in the cabinet to remove any residual trace impurities. A three-legged saturator is used for saturated vapor delivery. It is held at constant temperature using a recirculating chiller. An Isco syringe pump is used to deliver liquids. The liquid feed is vaporized using a temperature-regulated vortex mixer. The total pressure in the reactor is established using a back pressure controller. Pressure transducers are used to monitor the pressure of the feed, and the reactor pressure. All of the components are controlled using Lab View-based automation software and FieldPoint distributed I/O

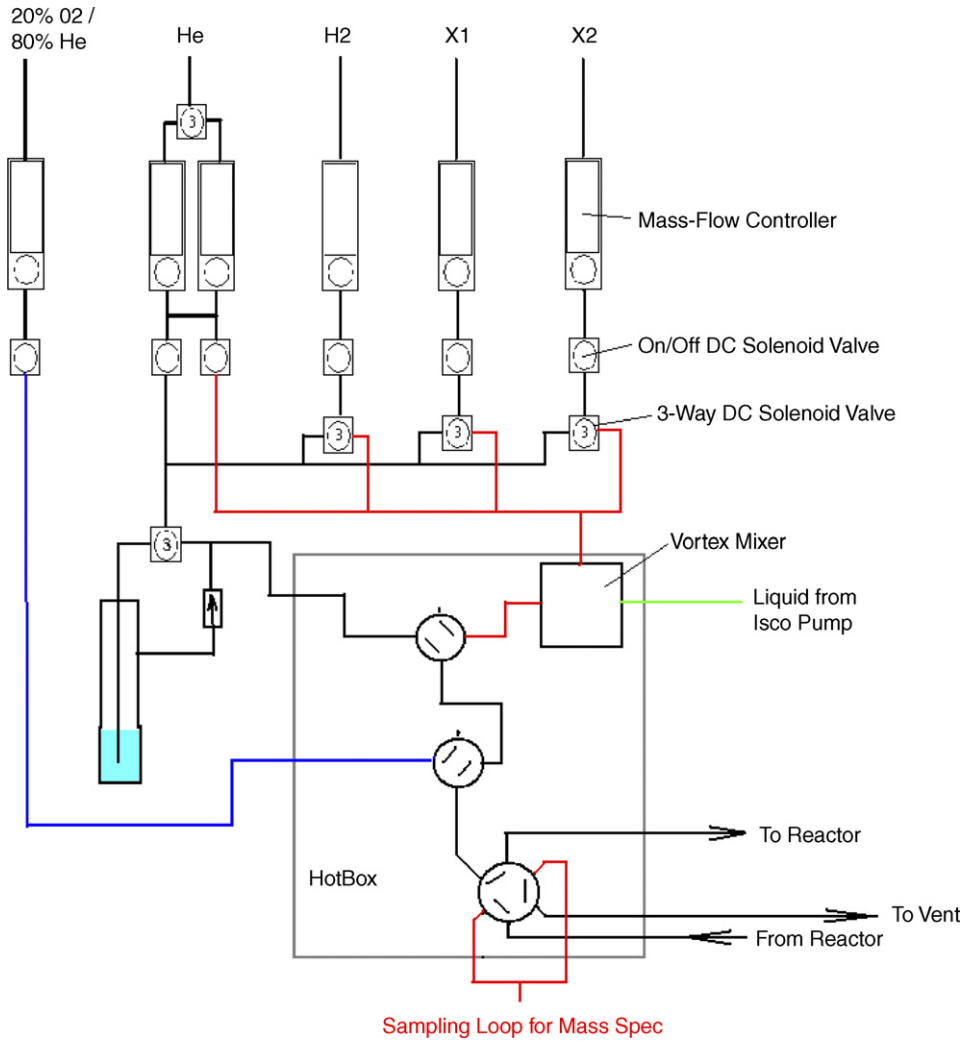

Fig. 4. Schematic of the gas/liquid feed system to the reactor showing the major components.

hardware. It is important to note from a safety perspective that the valving is designed to ensure that flammable gases or liquids cannot be mixed with the oxidant (typically 20% oxygen in helium). This is accomplished using an automated, timed, helium purge. All appropriate safety devices are incorporated into the design (e.g. relief valves and check valves).

The product exiting the reactor can be analyzed using any appropriate on-line analyzer (e.g. gas chromatograph, FTIR, or mass spectrometer). By the use of six-way Valco valves either the feed or the product can be sent to the on-line analyzer. In this manner the conversion and selectivity of the catalyst under test can readily be determined. In a typical arrangement the exit gas is sampled either using a Hiden quadrupole mass spectrometer (HPR-20) or a Varian micro-GC with appropriate column. While we have not conducted a burst pressure test of one of the beryllium tubes, they are rated at 5000 psig (341 bar) and XAFS data could theoretically be conducted at this pressure using this design. In practice, due to the solenoid valves currently installed, the present design is limited to maximum operating pressure of 100 psig (8 bar), but with higher pressure rated valves this limit could easily be exceeded.

3. Results and discussion

3.1. The cell as a catalytic micro-reactor

Prior to using the Be tube cell at the synchrotron it was tested as a catalytic micro-reactor in the laboratory at UOP. The reactor, with its temperature control, thermocouple, and heating, was connected to a standard laboratory micro-reactor pilot plan used for the dehydrogenation of methylcyclohexane (MCH) to toluene. A standard Pt–Sn/γ-Al_2O_3 reforming catalyst was reduced in 100% H_2 then cooled to 300 °C for the start of the activity testing. The MCH/H_2 at fixed ratio was fed to the reactor by passing the hydrogen through a saturator containing MCH held at constant temperature. Two injections of the product to the GC are made at each temperature (300–500 °C in 50 °C increments). The species monitored by the GC are MCH, toluene, benzene, and cyclohexane (methane and other cracked products are not measured). An empty beryllium tube was tested first, and showed $\ll$1% conversion of the MCH at temperatures up to 500 °C, indicating that the beryllium is inert under these reaction conditions. The overall conversion and selectivity to toluene for this catalyst run at comparable conditions in both a

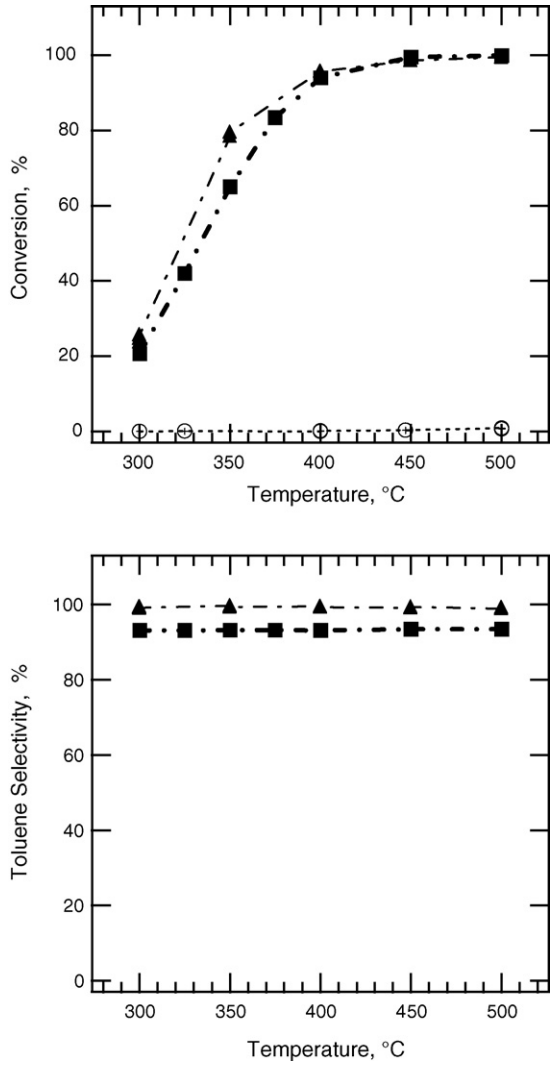

Fig. 5. A comparison of the methyl cyclohexane conversion (top) and toluene selectivity (bottom) of a standard laboratory micro-reactor with that of the Be tube reactor using a Pt–Sn/γ-Al_2O_3 catalyst as a function of temperature. Be tube reactor, filled triangles; micro-reactor, filled squares; empty Be tube reactor, empty circles. The toluene selectivity is defined as 100× (wt.% toluene/total conversion).

standard laboratory micro-reactor and in the beryllium tube reactor are shown in Fig. 5. Activity data from the empty rector are also displayed. As expected both the conversion profile and the selectivity profile are comparable for both the Be tube and laboratory micro-reactor. Thus the goal of having an in situ XAFS reactor design that exhibits the same selectivity and conversion at equivalent residence times to a laboratory micro-reactor has been met with this design for the typical catalytic reactions tested here. While this is an admirable goal there are some limitations with this configuration. Using a horizontal X-ray beam width that is similar in size to the depth of the catalyst bed implies that the XAFS data will be an average of all of the catalyst in the reactor. At high conversions the concentration of the feed and products will vary axially along the catalyst bed. If the gas phase composition affects the structure of the catalyst then this will be masked by the averaging over the length of the catalyst bed. The ideal manner in which to operate this reactor is therefore in differential conversion. However, recent in situ XAFS studies of high conversion processes using capillary-type reactors have been published. In these studies the structure of the active catalyst was spatially probed (either in 1D or 2D) and detailed information obtained on the axial variation of the catalyst structure [18,35–36]. Similar 1D or 2D imaging could be conducted using the reactor described here.

3.2. In situ XAFS

To demonstrate the capability of the in situ XAFS cell we show examples of in situ XAFS data from two different catalysts: (i) a 0.7 wt.% Re on γ-Al_2O_3/MOR catalyst where the equipment was used to determine the reduction kinetics as a function of hydrogen pressure, and (ii) a Pt–Sn/γ-Al_2O_3 reforming catalyst where true operando XAFS data were recorded during the reforming of *n*-heptane.

The effect of total hydrogen pressure on the reduction kinetics of the rhenium in a 0.7 wt.% Re/MOR/Al_2O_3 catalyst was studied in situ by recording the Re L_3-edge XANES as a function of hydrogen partial pressure. One hundred twenty milligram of 100–120 mesh catalyst was loaded into the reactor resulting in a bed depth of ∼20 mm. An X-ray horizontal beam size of 8 mm was used. This was centered onto the middle of the catalyst bed, thus the average over most of the bed was probed. The catalyst was dried in situ at 525 °C in a flow of 20% O_2/He. The flow rates were set at 50 cm^3/min for all of the experiments and were controlled by mass-flow controllers. The sample was reduced in a flow of hydrogen at three different hydrogen partial pressures (0.05 bar, 1.1 bar, and 7.9 bar). Pressures higher than the normal system pressure (1.1 bar) are maintained using a downstream pressure controller (Brooks model 5866). Fig. 6 shows a set of the Re L_3-edge XANES during reduction in 8 bar of hydrogen as the temperature is ramped at 4°/min to 500 °C. The temperature difference between each scan is approximately 30 °C. It has been shown that the position of the Re L_3-edge is a linear function of the Re oxidation state [37,38]. Thus, by

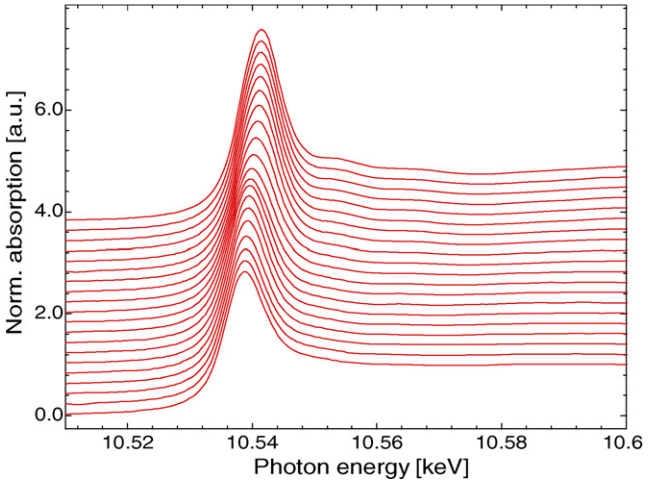

Fig. 6. Re L_3-edge TPR-XANES spectrum of the 0.7 wt.%Re/γ-Al_2O_3 catalyst as it is reduced at 7 bar H_2. The catalyst was ramped at 5°/min to 500 °C. The spectra are offset vertically for clarity. The temperature between each spectrum is 30 °C.

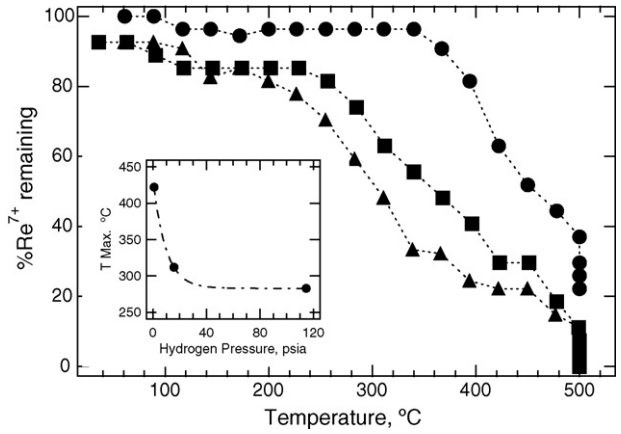

Fig. 7. Percentage of remaining oxidized rhenium for the 0.7 wt.% Re/γ-Al_2O_3/MOR catalyst as a function of temperature for three different hydrogen partial pressures (solid circles 0.05 bar, solid squares 1.1 bar, and solid triangles 7.9 bar). Inset shows the temperature of the maximum rate of reduction of the rhenium for the 0.7 wt.% Re/γ-Al_2O_3/MOR catalyst as a function of hydrogen partial pressure.

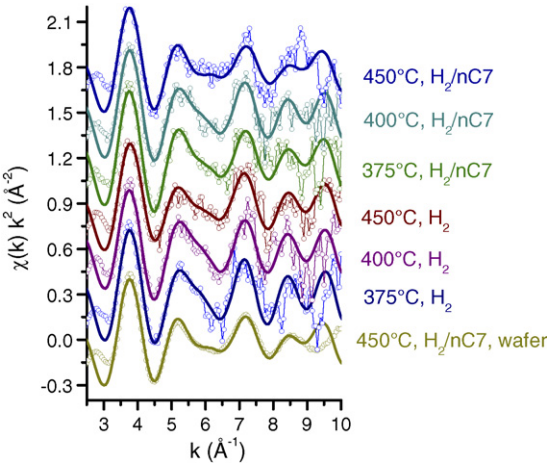

Fig. 8. The Pt L_3-edge $k^2\chi(k)$ plot for the Pt/Sn catalyst recorded at the given temperature in either hydrogen or H_2/nC_7. The data are the open circles and the best fit to the data the solid lines.

simply determining the position of the edge (using the inflection point) it is possible to convert the edge energy to the average rhenium oxidation state. In this manner it is possible to calculate the percentage of Re^{7+} remaining as a function of reduction temperature. Fig. 7 shows the percentage of oxidized rhenium remaining as a function of temperature for the three different hydrogen pressures. The temperature corresponding to the maximum rate of reduction is then plotted versus the hydrogen pressure in the inset of Fig. 7. There is a strong hydrogen pressure effect at low hydrogen pressures, but essentially zero dependence between 1 and 8 bar. While standard laboratory TPR techniques could be used to generate the reduction information at low hydrogen partial pressure [23] XAFS is an ideal characterization technique that can be used to obtain this information in situ at higher hydrogen pressure. It has been suggested that the nucleation of reduced Re atoms is the rate-determining step in the reduction of the perrhenate to metallic rhenium [23]. Faster nucleation may be obtained using a higher hydrogen pressure, but eventually the effect will saturate and thus increasing the hydrogen pressure will no longer affect the temperature of reduction, as shown in Fig. 7 (inset) above 3 bar.

3.3. In situ XAFS during catalysis

In order to demonstrate the full capabilities of the reactor, the Pt L_3-edge XAFS of a Pt–Sn/γ-Al_2O_3 catalysts was recorded in situ while the catalyst was being used to reform *n*-heptane. In this example 75 mg of a 100/120 mesh sample of the Pt–Sn/γ-Al_2O_3 catalyst was loaded into the 3.5 mm OD Be tube, giving a bed depth of ∼13 mm. A horizontal X-ray beam size of 8 mm, centered on the catalyst bed, was used so that the average structure of the catalyst in the reactor is probed. The catalyst was first reduced in situ in hydrogen prior to the reforming catalysis. A hydrogen-to-hydrocarbon ratio of 66 was achieved by flowing 25 cm^3/min hydrogen through a saturator filled with *n*-heptane held at constant temperature. Pt L_3-edge EXAFS data were recorded both in 100% hydrogen and in the H_2/*n*-heptane feed at three different temperatures: 375, 400, and 450 °C. Fig. 8 shows a comparison of the Pt L_3-edge $k^2\chi(k)$ data recorded in pure hydrogen with those recorded in the H_2/*n*-heptane at each of the three temperatures. Clearly the EXAFS data is of lower quality than that for the rhenium-based catalysts, but even with this signal/noise there is information to be gained (see below). It is also interesting to compare the in situ EXAFS data obtained from a pressed wafer of the same Pt–Sn/γ-Al_2O_3 catalyst with the same absorption length (obtained using the cell design in Ref. [6]) at 450 °C in H_2/nC_7 with that obtained using the Be tube reactor. This comparison is also shown in Fig. 8. Clearly the signal/noise ratio is significantly improved in this data set relative to the equivalent data set using the Be tube reactor. We believe that the major reason for lower signal quality in the Be tube data is the fact that a meshed catalyst is being used versus a uniform pressed wafer. This will be explored in more detail in a subsequent publication.

Nevertheless the operando Pt L_3-edge EXAFS data can be modeled with Pt–O, Pt–Pt and Pt–Sn scattering paths. The results of the fit and the goodness-of-fit parameter (*R*-factors) are listed in Table 1. The model is reasonable for the measured spectra as indicated by the *R*-factor values of 0.1–2.0%. The data series consisting of the two different atmospheres and three different temperatures (375 °C, 400 °C, and 450 °C) were simultaneously modeled along with a 450 °C H_2/nC_7 spectrum from the pressed wafer of higher quality. The data were modeled over the data range starting at 3.3 $Å^{-1}$ and extending to 7–9 $Å^{-1}$, as allowed by the data quality. The EXAFS model consists of three scattering paths, Pt–O, Pt–Pt, and Pt–Sn. Due to the low quality of the EXAFS spectra the temperature dependence of σ^2 was found to be within the experimental uncertainty. Also the temperature and/or atmospheric dependence of the bond length (ΔR) to the three neighboring atoms were not distinguishable. Therefore, all seven spectra were modeled with one bond length and one σ^2 value for each of the three (Pt–O, Pt–Pt, and Pt–Sn) signals. The number of neighboring atoms was determined independently for each

Table 1
Structural parameters determined in situ for the Pt/Sn/γ-Al_2O_3 catalyst

Data set	Path	N	R (Å)	σ^2 ($\times 10^{-3}$ Å^2)	R-factor (%)
450H_2/nC_7 wafer	Pt–O	0.2 ± 0.1	1.67 ± 0.02	5.4 ± 5.1	0.1
375H_2		0.1 ± 0.1			1.4
400H_2		0.0 ± 0.0			1.7
450H_2		0.3 ± 0.1			2.0
375H_2/nC_7		0.1 ± 0.1			0.2
400H_2/nC_7		0.1 ± 0.1			1.9
450H_2/nC_7		0.2 ± 0.1			1.5
450H_2/nC_7 wafer	Pt–Pt	3.3 ± 0.3	2.64 ± 0.00	7.1 ± 1.8	
375H_2		4.4 ± 0.5			
400H_2		4.0 ± 0.5			
450H_2		3.6 ± 0.5			
375H_2/nC_7		4.0 ± 0.4			
400H_2/nC_7		4.0 ± 0.5			
450H_2/nC_7		3.1 ± 0.4			
450H_2/nC_7 wafer	Pt–Sn	1.8 ± 0.2	2.52 ± 0.01	8.7 ± 2.6	
375H_2		1.6 ± 0.2			
400H_2		1.6 ± 0.3			
450H_2		1.5 ± 0.3			
375H_2/nC_7		2.0 ± 0.3			
400H_2/nC_7		1.7 ± 0.3			
450H_2/nC_7		1.8 ± 0.3			

N is the coordination number, R the distance, and σ^2 is the Debye–Waller factor.

spectrum. In addition one energy shift value (ΔE_0) was determined from the model. The value for $S_0{}^2$ is 0.91 ± 0.05 as determined from Pt-foil. Therefore, there were seven common parameters (σ^2 o, σ^2 pt, σ^2 sn, ΔR o, ΔR pt, ΔR sn, ΔE_0) and three independent parameters (No, Npt, and Nsn) for an average of four parameters/data set (seven common parameters/seven data sets plus three independent parameters). The similarity in the coordination numbers listed in Table 1 show that within the accuracy of these measurements there is no difference in the Pt–Sn cluster chemistry (average cluster size and average Pt/Sn stoichiometry) with the catalyst in pure hydrogen versus in the H_2/nC_7 feed. The Pt–Pt and Pt–Sn bond lengths reported in Table 1 are comparable with studies in the literature [24,25]. Meitzner et al. report a Pt–Pt distance of 2.75 Å and Pt–Sn bond length of 2.61 Å, while Caballero et al. report bond lengths of 2.68 Å for Pt–Pt and 2.93 Å for Pt–Sn. Both of these studies were recorded at low temperature after cooling the sample in a flow of hydrogen. Our data has the Pt–Sn bond length (2.52 ± 0.01) shorter than the Pt–Pt bond length (2.64 ± 0.00) in agreement with Meitzner et al. but both of our bond lengths are significantly shorter than those of Meitzer et al. Contraction of the Pt–Pt bond length in small clusters is well known in the literature, and that it relaxes towards the bulk value (2.774 Å) when H is chemisorbed [39–41]. In our experiments there will

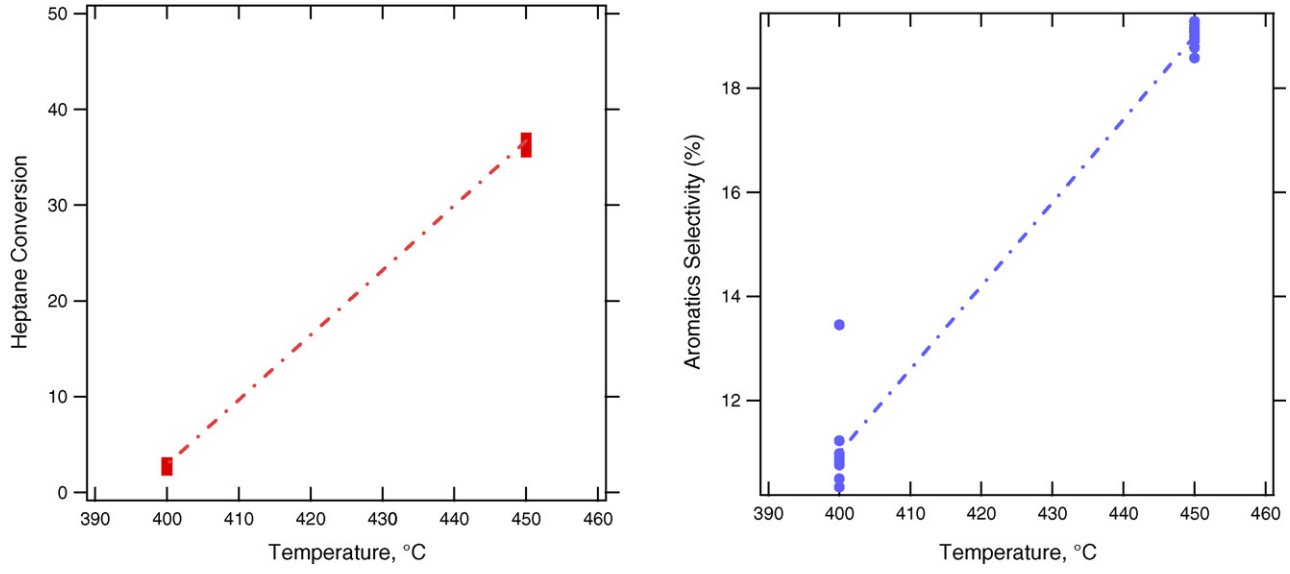

Fig. 9. The heptane conversion (left) and aromatics selectivity (right), as a function of temperature measured simultaneously with the Pt L_3-edge EXAFS data shown in Fig. 8. The aromatics selectivity is defined as 100× (wt.% sum of all aromatics/total conversion). The sum of aromatics is the sum of benzene and toluene.

be no significant steady-state coverage of hydrogen (the lowest temperature data were recorded was 375 °C). Thus, it would be expected that the bond lengths would then resemble those of an H-free cluster [39–41]. For a neutral Pt atom and a neutral Sn atom the predicted bond length would be 2.80 Å. The fact that we measure a Pt–Sn bond length shorter than that for Pt–Pt is an indication that the Sn is not fully reduced [24]. Although, improvements to the sample preparation methods are needed for this catalyst to improve the quality of the EXAFS signal, many aspects of the cell design are demonstrated. On-line GC data were recorded while the EXAFS data were being measured. The heptane conversion and the aromatics selectivity of this catalyst are plotted as a function of reaction temperature in Fig. 9. We believe that these initial results – simultaneous EXAFS and GC at realistic catalytic conditions of temperature, pressure and contact time – are encouraging enough that this experimental arrangement will lead to important understanding of many catalytic systems.

4. Summary

We have demonstrated the design and initial operation of a versatile capillary-type in situ transmission XAFS reactor fabricated from beryllium. This reactor allows true operando XAFS data to be recorded. The overall experimental arrangement of the Be tube cell, gas feed system, and on-line analysis is able to provide high quality in situ XAFS data. This reactor design has already provided useful XAFS data to be recorded that has supported both true R&D activities at UOP, and also helped support commercial catalyst development issues. This reactor can be used over a wide process variable range and range of X-ray energies for a wide array of heterogeneous catalysts.

Acknowledgements

Jenia Karapetrova is thanked for help and guidance at 33BM. Research carried out in part at the National Synchrotron Light Source, Brookhaven National Laboratory, which is supported by the U.S. Department of Energy, Division of Materials Sciences and Division of Chemical Sciences, under Contract No. DE-AC02-98CH10886. Use of the Advanced Photon Source was supported by the U.S. Department of Energy, Office of Science, Office of Basic Energy Sciences, under Contract No. W-31-109-Eng-38.

References

[1] J.W. Niemanstsverdriet, Spectroscopy in Catalysis—An Introduction, Wiley-VCH, Weinheim, 2000.
[2] J.M. Thomas, W.J. Thomas, Principles and Practice of Heterogeneous Catalysis, VCH, Weinheim, 1997.
[3] R.A. van Santen, Theoretical Heterogeneous Catalysis, World Scientific, Singapore, 1991.
[4] B.M. Weckhuysen, Chem. Comm. 58 (2002) 97.
[5] A.M. Argo, J.F. Odzak, F.S. Lai, B.C. Gates, Nature 315 (2002) 623.
[6] S.R. Bare, G.E. Mickelson, F.S. Modica, A.Z. Ringwelski, N. Yang, Rev. Sci. Instrum. 77 (2006) 023105.
[7] G. Meitzner, S.R. Bare, D. Parker, H. Woo, D.A. Fischer, Rev. Sci. Instrum. 69 (1998) 2618.
[8] J.-D. Grunwaldt, M. Caravati, S. Habnnemann, A. Baiker, Phys. Chem. Chem. Phys. 6 (2004) 3037.
[9] B.S. Clausen, G. Steffensen, B. Fabius, J. Villadsen, R. Friedhans'l, H. Topsoe, J. Catal. 132 (1991) 524.
[10] B.S. Clausen, H. Topsoe, Catal. Today 9 (1991) 189.
[11] R.E. Jentoft, S.E. Deutch, B.C. Gates, Rev. Sci. Instrum. 67 (1996) 2111.
[12] G. Meitzner, E. Iglesia, Catal. Today 53 (1999) 433.
[13] M.S. Nashner, A.I. Frenkel, D.L. Adler, J.R. Shapley, R.G. Nuzzo, J. Am. Chem. Soc. 119 (1997) 7760.
[14] R.A. Dalla Betta, M. Boudart, K. Foger, D.G. Loffler, J. Sanchez-Arrieta, Rev. Sci. Instrum. 55 (1984) 1910.
[15] F.W.H. Kampers, T.M.J. Maas, J. van Grondelle, P. Brinkgrave, D.C. Koningsberger, Rev. Sci. Instrum. 60 (1989) 2635.
[16] (a) G. Meitzner, E. Igelsia, Catal. Today 53 (1999) 433;
(b) D.G. Barton, S.L. Soled, G.D. Meitzner, G.A. Fuentes, E. Igelsia, J. Catal. 181 (1999) 57.
[17] M.A. Newton, A.J. Dent, S. Diaz-Moreno, S.G. Fiddy, B. Jyoti, J. Evans, Chem. Eur. J. 12 (2006) 1975.
[18] M.A. Newton, F.G. Fiddy, G. Guilera, B. Jyoti, J. Evans, Chem. Comm. (2005) 118.
[19] For information on the properties of Kapton® see http://www2.dupont.com/Kapton/en_US/assets/downloads/pdf/summaryofprop.pdf.
[20] B. Mitra, X. Gao, I.E. Wachs, A.M. Hirt, G. Deo, Phys. Chem. Chem. Phys. 3 (2001) 1144.
[21] A.S. Fung, P.A. Tooley, M.J. Kelley, D.C. Koningsberger, B.C. Gates, J. Phys. Chem. 95 (1991) 225.
[22] P. Arnoldy, E.M. van Oers, O.S.L. Bruinsma, V.H.J. De Beer, J.A. Moulijn, J. Catal. 93 (1985) 231.
[23] C. Bolivar, H. Charcosset, R. Frety, M. Primet, L. Tournayan, C. Betizeau, C. Leclerq, R. Maurel, J. Catal. 39 (1975) 249.
[24] G. Meiztner, G.H. Via, F.W. Lytle, S.C. Fung, J.H. Sinfelt, J. Phys. Chem. 92 (1998) 2925.
[25] A. Caballero, H. Dexpert, B. Didillon, F. LePeltier, O. Clause, J. Lynch, J. Phys. Chem. 97 (1993) 11283.
[26] A. Borgna, S.M. Stagg, D.E. Resasco, J. Phys. Chem. B 102 (1998) 5077.
[27] B. Ravel, M. Newville, J. Synch. Rad. 12 (2005) 537.
[28] M. Newville, J. Synch. Rad. 8 (2001) 322.
[29] S.I. Zabinsky, J.J. Rehr, A. Ankudinov, R.C. Albers, M.J. Eller, Phys. Rev. B. 52 (1995) 2995.
[30] PF-60 grade beryllium contains up to 800 ppm Fe, and other trace elements. Therefore, this may limit the use of this reactor for certain applications. For details on the properties of beryllium, and the different grades available see: http://www.brushwellman.com.
[31] For detailed environmental safety and health information on beryllium see http://www.brushwellman.com.
[32] T. Murata, K. Nakagawa, A. Kimura, N. Otoda, I. Shimoyana, Rev. Sci. Instrum. 66 (1995) 1437.
[33] J.-D. Grunwaldt, M. Caravati, M. Ramin, A. Baiker, Catal. Lett. 90 (2003) 221.
[34] J.-D. Grunwaldt, M. Ramin, M. Rohr, A. Michailovski, G.R. Patzke, A. Baiker, Rev. Sci. Instr. 76 (2005) 054104.
[35] J.-D. Grunwaldt, A. Baiker, Catal. Lett. 99 (2005) 5.
[36] J.-D. Grunwaldt, S. Hannemann, C.G. Schroer, A. Baiker, J. Phys. Chem. B 110 (2006) 8674.
[37] F.W. Lytle, P.S.P. Wei, R.B. Greegor, G.H. Via, J.H. Sinfelt, J. Chem. Phys. 70 (1979) 4849.
[38] N. Yang, G.E. Micklelson, F.S. Modica, E. Boldingh, S.R. Bare, S.D. Kelly, F.D. Vila, J. Kas, J.J. Rehr, J. Phys. Chem. B, submitted for publication.
[39] S.N. Reifsnyder, M.M. Otten, D.E. Sayers, H.H. Lamb, J. Phys. Chem. B 101 (1997) 4972.
[40] M. Vaarkamp, J.T. Miller, F.S. Modica, D.C. Koningsberger, J. Catal. 163 (1996) 294.
[41] A.L. Ankudinov, J.J. Rehr, J.J. Low, S.R. Bare, J. Chem. Phys. 116 (2002) 1911.